HHS Public Access

Author manuscript

Neuroscience. Author manuscript; available in PMC 2018 March 06.

Published in final edited form as:

Neuroscience. 2017 March 06; 344: 380–393. doi:10.1016/j.neuroscience.2016.12.055.

Conditional deletion of pejvakin in adult outer hair cells causes progressive hearing loss in mice

Suzan L. Harris[1], **Marcin Kazmierczak**[1], **Tina Pangrši**[2], **Prahar Shah**[1], **Nadiya Chuchvara**[1], **Alonso Barrantes-Freer**[2,#], **Tobias Moser**[2], and **Martin Schwander**[1,*]

[1]Department of Cell Biology and Neuroscience, Rutgers the State University of New Jersey, Piscataway, New Jersey 08854

[2]Institute for Auditory Neuroscience and InnerEarLab, University Medical Center Göttingen, 37099 Göttingen, Germany; Collaborative Research Center 889, University of Göttingen, 37099 Göttingen, Germany

Abstract

Mutations in the *Pejvakin* (*Pjvk*) gene cause autosomal recessive hearing loss DFNB59 with audiological features of auditory neuropathy spectrum disorder (ANSD) or cochlear dysfunction. The precise mechanisms underlying the variable clinical phenotypes of DFNB59 remain unclear. Here, we demonstrate that mice with conditional ablation of the *Pjvk* gene in all sensory hair cells or only in outer hair cells (OHCs) show similar auditory phenotypes with early-onset profound hearing loss. By contrast, loss of *Pjvk* in adult OHCs causes a slowly progressive hearing loss associated with OHC degeneration and delayed loss of inner hair cells (IHCs), indicating a primary role for pejvakin in regulating OHC function and survival. Consistent with this model, synaptic transmission at the IHC ribbon synapse is largely unaffected in *sirtaki* mice that carry a C-terminal deletion mutation in *Pjvk*. Using the C-terminal domain of pejvakin as bait, we identified in a cochlear cDNA library ROCK2, an effector for the small GTPase Rho, and the scaffold protein IQGAP1, involved in modulating actin dynamics. Both ROCK2 and IQGAP1 associate via their coiled-coil domains with pejvakin. We conclude that pejvakin is required to sustain OHC activity and survival in a cell-autonomous manner likely involving regulation of Rho signaling.

Keywords

Auditory neuropathy; inner ear; DFNB59; pejvakin; hearing loss; hair cell

[*]Corresponding author: Rutgers the State University of New Jersey, 604 Allison Road, Piscataway, NJ 08854, Phone: 848-445-2709, schwander@biology.rutgers.edu.

[#]present address: Institute of Neuropathology, University Medical Center Göttingen, 37099 Göttingen, Germany

Introduction

Hair cells of the mammalian inner ear are highly specialized mechanosensors that convert mechanical stimuli into electrical impulses. There are two types of hair cells in the organ of Corti, the sensory epithelium of the cochlea, that have different morphological and physiological properties and subserve unique functions (Dallos, 1992). IHCs are the true sensory cells that transmit the electrical signals via specialized ribbon synapses to the auditory nerve (Wichmann and Moser, 2015), whereas OHCs act as mechanical amplifiers that enhance weak sounds in the cochlea and are regulated by efferent input from the brainstem (Warr and Guinan, 1979; Zheng et al., 2000; Liberman et al., 2002; Dallos et al., 2008). Much remains to be known about the molecular mechanisms that control the morphological and functional specialization of these two types of hair cells and maintain their integrity throughout life.

Sensorineural hearing loss is frequently caused by defects in OHCs that seem more susceptible to damage by noise and genetic perturbations than IHCs. By contrast, mutations in only a few genes disrupt IHC function, without directly compromising OHC activity, including otoferlin (OTOF), SLC17A8 (encoding the vesicular glutamate transporter-3 (VGLUT3)), and Diaphanous homolog 3 (DIAPH3) (Varga et al., 2003; Roux et al., 2006; Ruel et al., 2008; Schoen et al., 2010). Patients carrying mutations in these genes often present with an abnormal auditory brainstem response (ABR), indicative of IHC dysfunction, but preserved otoacoustic emissions (OAEs), reflecting normal OHC activity, and therefore meet the diagnostic criteria for ANSD (Starr et al., 1996; Kemp, 2002b; Moser and Starr, 2016). ANSD is caused by defects in the encoding and processing of sound at IHCs, the IHC synapse, or the auditory nerve itself. While mutations in the OTOF and SLC17A8 genes cause defects at the IHC synapse (also termed auditory synaptopathy) (Roux et al., 2006; Ruel et al., 2008), DIAPH3 is critical for the long-term maintenance of IHC stereocilia and possibly synapses (Schoen et al., 2010). Thus, while only few genetic forms of ANSD are known, they have mostly been attributed to defects at the IHC synapse. More complex mechanisms may contribute to DFNB59, an autosomal recessive form of hearing loss that can manifest as ANSD or cochlear deafness (Delmaghani et al., 2006; Collin et al., 2007a; Schwander et al., 2007b). Two missense mutations (p.T54I and p.R183W) in *Pjvk* were initially reported in DFNB59 patients with audiological hallmarks of ANSD including abnormal ABR and preserved OAEs (Delmaghani et al., 2006). Evidence suggests that these mutations affect the conduction of signals in the auditory nerve, while leaving OHC function unaffected (Delmaghani et al., 2006). However, subsequent studies identified *Pjvk* nonsense mutations in DFNB59 patients with progressive hearing loss and, in many cases, absent OAEs (Chaleshtori et al., 2007; Collin et al., 2007b; Ebermann et al., 2007; Schwander et al., 2007a; Zhang et al., 2015). Importantly, abnormal OAEs have also been reported in individuals carrying the ANSD-linked p.R183W mutation (Collin et al., 2007b), raising the question of whether OHC defects may secondarily develop over time as the disease progresses and whether DFNB59 meets the diagnostic criteria of ANSD.

Pejvakin is a distantly-related member of the gasdermin family of genes (Saeki et al., 2000). All gasdermins share a common N-terminal gasdermin (GSDM) domain. The GSDM N-

domain of some gasdermins bears intrinsic cytotoxic activity (Op de Beeck et al., 2011; Shi et al., 2015), although no such function has been reported for the GSDM N-domain of pejvakin. The C-terminal domain of pejvakin bears homology with Zinc binding proteins, and its deletion causes progressive hearing loss and abnormal OAEs in the ENU-induced *sirtaki* mouse line (Schwander et al., 2007a), suggesting a critical role for the C-terminal domain in pejvakin function. A recent study suggested a possible role for pejvakin in regulating peroxisome proliferation in sensory hair cells and auditory neurons in response to oxidative stress (Delmaghani et al., 2015), although no peroxisomal targeting sequence has been detected in its primary sequence. Thus, clarification of the mechanisms underlying the phenotypic variability associated with mutations in the *Pjvk* gene awaits identification of its molecular and cell-type specific functions.

To determine the extent to which pejvakin regulates the development and maintenance of IHCs and OHCs, we have carried out targeted disruption of the *Pjvk* gene in the early postnatal and adult cochlea. Here, we report that genetic ablation of pejvakin in all cochlear hair cells or only in OHCs leads to an early-onset profound hearing loss. Pejvakin is also required to sustain the activity and survival of OHCs in the adult cochlea but is largely dispensable for synaptic transmission at the IHC ribbon synapse. Using yeast two-hybrid screens of a cochlear cDNA library, we identified ROCK2 and IQGAP1, well-known regulators of actin dynamics, as binding proteins for pejvakin (Mateer et al., 2002; Shimizu et al., 2003; Brown and Sacks, 2006; Truebestein et al., 2015). Our findings show that loss of function mutations in *Pjvk* affect OHC function in an age-dependent manner, possibly by compromising the integrity of the hair cell cytoskeleton.

Experimental Procedures

Mouse strains, ABR and DPOAE measurements

All procedures were performed in accordance with research guidelines of the institutional animal care and use committee of Rutgers University. Mice of either sex were studied. The measurement of ABRs and distortion product otoacoustic emissions (DPOAEs) was carried out as described (Schwander et al., 2007a). tdTomato reporter mice (B6.Cg-Gt(ROSA)26Sor$^{tm9(CAG\text{-}tdTomato)Hze}$/J) and wild-type C57BL6 mice were obtained from The Jackson Laboratory. *Atoh1-CreER™* (Chow et al., 2006) and *Prestin-CreER*^{T2} (Fang et al., 2012) mice were a kind gift from S. Baker and J. Zuo (St. Jude Children's Research Hospital, Memphis, TN), respectively. Generation of pejvakin floxed mice (*Pjvk*$^{fl/fl}$) mice will be described in detail elsewhere (M. Kazmierczak, P. Kazmierczak, A.W. Peng, S.L. Harris, P. Shah, J.-L. Puel, M. Lenoir, S.J. Franco, and M. Schwander, unpublished observations). *Pjvk*$^{fl/fl}$ mice were crossed with *Atoh1-CreER™* and Prestin-*CreER*^{T2} mice and genotyped as previously described (Graus-Porta et al., 2001). Double heterozygous *Pjvk*$^{fl/+}$*; Atoh1-CreER™* and *Pjvk*$^{fl/+}$*; Prestin-CreER*^{T2} mice were crossed with homozygous *Pjvk*$^{fl/fl}$ mice to obtain animals used in experiments. To induce Cre activity in crosses with *Atoh1-CreER™* mice, pups were intraperitoneally (IP) injected once daily with tamoxifen (T5648, Sigma) dissolved in corn oil (C8267, Sigma) at a dose of 3mg/40g body weight at P0 and P1. To induce Cre activity in crosses with *Prestin-CreER*^{T2} mice, pups were injected IP once daily either at P2-P4 with 3mg/40g or at P21 and P22 with 9 mg/40g

body weight. *Pjvk* conditional knockout (KO) mice were genotyped for the presence of Cre recombinase and the pejvakin floxed allele. Detection of Cre allele: Cre_fw GACATGTTCAGGGATCGCCAGGCG, Cre_rv1 GACGGAAATCCATCGCTCGACCAG; Detection of Flox allele: FloxLongfw GAATTCCTCTTGGATGATGGCCACTGCAGA, FloxLongrv AACGAAGCTCTTGGTAGCAGCAGCAAACAT. *Sirtaki* mice were genotyped as previously described (Schwander et al., 2007b).

Histology and immunohistochemistry

Inner ear sections were stained with hematoxylin and eosin as described (Schwander et al., 2007b). Whole mount staining of cochlear sensory epithelia with anti-myosin VIIa (rabbit; Proteus Biosciences) and 488-phalloidin (Life Technologies) were carried out as described (Senften et al., 2006; Schwander et al., 2007b). The whole mount preparations were imaged with a BX63 fluorescence microscope (Olympus). Hair cells were counted as present if myosin VIIa-positive cell bodies and V-shaped hair bundles were intact. CellSense software (Olympus) was used to measure the total length of cochlear whole mounts and the length of individual counted segments. The total number of IHCs and OHCs was counted in each of three cochlear segments (apical, medial and basal) of 600–1600 μm. Density (cells per 100 μm) of hair cells was then calculated for each segment.

Immunohistochemistry for CtBP2 and GluR2/3 was performed as described previously (Khimich et al., 2005). In brief, the organs were fixed with 4% formaldehyde for 10 minutes on ice, immunolabeled by mouse IgG1 anti-CtBP2 (BD Biosciences, 1:200) and rabbit anti-GluR2/3 (Chemicon, 1:200) primary antibodies and secondary AlexaFluor488- and AlexaFluor568-labeled antibodies (Molecular Probes, 1:200). Confocal images were acquired using a laser scanning confocal microscope (Leica TCS SP2, Leica Microsystems CMS GmbH, Mannheim, Germany) with 488 nm (Ar) and 561 nm (He-Ne) lasers and a 60× oil immersion objective. Z-axis stacks of 2D images were taken with a step size of 0.5 μm. Z-projections and analysis were done in ImageJ. The ribeye/CtBP2 and GluR2/3 immunofluorescence spots were counted in the z-stacks and divided by the number of IHCs. Juxtaposed spots of pre- and postsynaptic immunofluorescence were taken to identify intact IHC ribbon synapses.

In addition, HeLa cells were co-transfected with an expression vector (pcDNA3.1, Clontech) encoding the N-terminal gasdermin domain (amino acids 1–239) or C-terminal domain (amino acids 241–352) of pejvakin fused to FLAG-epitope tag and pEGFP-IQGAP1. Protein expression was evaluated by immunofluorescence analysis with anti-GFP (rabbit; Abcam) and anti-Flag (mouse, Sigma) antibodies as described (Senften et al., 2006). Additional antibodies were as follows: Alexa Fluor 568 anti-rabbit and anti-mouse (Life Technologies), and Alexa Fluor 488–phalloidin (Life Technologies), and horseradish peroxidase-conjugated anti-rabbit (GE Healthcare).

DNA constructs, immunoprecipitation and western blot analysis

pEGFP-IQGAP1 was a kind gift from David Sacks (Addgene plasmid # 30112). HA-tagged ROCK2 (pXJ40 HA Rok-alpha) was a kind gift from Thomas Leung (Leung et al., 1996). HEK293 cells were transiently transfected using X-tremeGENE 9 DNA transfection reagent

(Roche) according to the manufacturer's instructions. Cell lysis, immunoprecipitations with anti-GFP antibody (rabbit, Sigma) or anti-Flag antibody (mouse, Sigma) and Western blot analysis were carried out as described (Kazmierczak et al., 2015), except that cellular extracts were prepared in 50 mM TrisHCl, pH 7.6, 150 mM NaCl, 1% NP-40 and immunocomplexes washed three times in 50 mM TrisHCl, pH 7.6, 150 mM NaCl, and 0.25% NP-40. The blots were probed with anti-GFP (rabbit, Sigma), anti-Flag (mouse, Sigma) and anti-HA-HRP (rat, Roche) antibodies. Primary antibodies and proteins were visualized with HRP-conjugated anti-rabbit antibody (1:20000, GE Healthcare) using the ECL2 detection system (Thermo Fisher Scientific).

Patch-clamp recordings

Recordings were performed in 2–3-week-old mice. The apical cochlear turns were dissected in HEPES Hank's solution containing (in mM): 5.36 KCl, 141.7 NaCl, 1 $MgCl_2$, 0.5 $MgSO_4$, 10 HEPES, 11.1 D-glucose and 3.42 L-glutamine, pH: 7.2. IHCs were patch-clamped in the perforated-patch configuration as previously described (Brandt et al., 2003). The pipette solutions contained (in mM): 130 Cs-gluconate, 10 TEA-Cl, 10 4-AP (4-aminopyridine; Merck KGaA, Darmstadt, Germany), 1 $MgCl_2$, 10 HEPES, 300 μg/ml amphotericin B (Calbiochem, La Jolla, CA), pH: 7.17, osmolarity: approx. 290 mOsm. The extracellular solutions contained (in mM): 113 NaCl, 35 TEA-Cl, 2.8 KCl, 2 $CaCl_2$, 1 $MgCl_2$, 10 HEPES, 1 CsCl, 11.1 D-glucose, pH: 7.2, osmolarity: approx. 300 mOsm). All chemicals were obtained from Sigma-Aldrich (St. Louis, MO). Recordings were done at room temperature with an EPC-9 amplifier (HEKA Electronics, Lambrecht, Germany) controlled by Pulse software (HEKA). Membrane capacitance increments (ΔC_m) were measured as previously described (Moser and Beutner, 2000), averaging 400 ms before and after (skipping the first 100 ms) depolarization. To measure ΔC_m, IHCs were stimulated by depolarizations of different durations to peak Ca^{2+} current potential at intervals of 30 to 60 s. For Ca^{2+} current inactivation experiments IHCs were depolarized for 100 ms. All voltages were corrected for liquid junction potential (-14 mV). Analysis of results from patch-clamp experiments was performed in Igor Pro (Wavemetrics, Eugene, OR) software. Current-voltage relationships were fitted with a custom made macro in Igor Pro: the reversal potential was estimated by fitting a line to the IV in the range of 20–40 mV (not corrected for the liquid junction potential). Conductance was calculated as $G(V)=I(V)/(V-V_{rev})$, where V is the test potential, V_{rev} is the estimated reversal potential, I(V) is the average current at V, and G is the conductance at V. Conductance traces were normalized and the normalized G trace was fitted with the Boltzmann equation $G(V)=G_{max}/(1+\exp((V_{half}-V)/slope)$, where V_{half} is potential of half activation. Data were tested for randomness, normality (*Jarque-Bera test*) and equality of variances (*F-test*) and compared for statistical significance using *Student's t test* or *Wilcoxon rank-sum test*, as appropriate.

Quantitative PCR

Reverse transcription and qPCR was performed as described previously (Kazmierczak et al., 2015). Primers recognizing *Pgk1* were: forward, 5′-CAACAACATGGAGATTGGCACA, reverse 5′-ACAGTAGCTTGGCCAGTCTTG; and for *Pjvk*: forward CGGTGCCTTCGACATTTGTG, reverse 5′-GCGTCCATCACTCTCCTGTT. No reverse transcriptase controls (no-RT controls) were included as negative controls for each sample

and primer pair to assess the levels of nonspecific amplification, as described previously (Kazmierczak et al., 2015).

Yeast two-hybrid screens

P4–P7 mouse cochlear cDNA library was a kind gift of Ulrich Muller (Zhao et al., 2014). Full length and C-terminal portion pejvakin (amino acids 239–352) were cloned into both LexA-N and LexA-C bait vectors (Dualsystems), which allow expression of N-and C-terminal LexA fusion proteins and carry a TRP1 auxotrophic marker. Both the DNA binding domain-bait and bait-DNA binding domain orientation were used to account for differences in case of self-activation of the reporter gene or improper folding of the bait protein. Bait plasmids were transformed into the NMY51 yeast reporter strain using LiAc methods. Yeast two-hybrid screens were performed according to the manufacturer's instructions (Dualsystems) and more than 10 million transformants were screened for each bait. The interactions between candidate clones and baits were verified by isolating and re-introducing the respective bait and prey plasmids into the NMY51 yeast strain. The transformants were reassessed by nutritional selection and X-α-gal plate assay as described in the manufacturer's instructions (Dualsystems).

Statistical analysis

Data analysis was performed using Igor Pro (Wavemetrics, Eugene, OR) and Excel (Microsoft, Redmond, WA) software. All data are mean ± standard error of the mean (SEM). Data were tested for randomness, normality (Jarque-Bera test) and equality of variances (F-test) and compared for statistical significance using Student's *t*-test or Wilcoxon rank-sum test, as appropriate (*$p < 0.05$, **$p < 0.01$, *** $p < 0.001$). The number "n" in each assay corresponds to the number of independent data points and is equal to the number of animals analyzed for each group. In all analysis, a Bonferroni test was used to correct for multiple comparisons.

Results

Pjvk is selectively expressed in sensory hair cells

Pejvakin was initially reported to be broadly expressed in hair cells, supporting cells, and different neuronal populations of the auditory pathway (Delmaghani et al., 2006). Recent studies based on a monoclonal antibody detected pejvakin in hair cells of the inner ear, while neuronal expression has not been reported (Delmaghani et al., 2015). To further define the expression pattern of pejvakin, we compared the relative levels of pejvakin mRNA, normalized to the housekeeping gene *Pgk1*, in different inner ear tissues at P5 by quantitative real-time PCR. Expression of *Pjvk* transcripts was more than three-fold higher in the organ of Corti when compared to stria vascularis ($p < 0.01$, two-tailed *t*-test) or modiolus ($p < 0.01$), which harbors spiral ganglion neurons (Fig. 1A). These findings are consistent with the hair cell-specific expression pattern of pejvakin in the Shared Harvard Inner-Ear Laboratory Database (https://shield.hms.harvard.edu). By in situ hybridization, we detected *Pjvk* expression in sensory hair cells (Fig. 1B and C, arrowheads) of the cochlea at postnatal (P) day 4 but not in spiral ganglion neurons (asterisks). No signal was observed in hair cells with a sense probe (Fig. 1D and E, arrowhead).

Since *Pjvk* mRNA is present in hair cells and OHC function is affected in some DFNB59 patients carrying the p.R183W mutation (Collin et al., 2007a), we hypothesized that pejvakin might be important for hair cell survival. To define the effect of pejvakin deficiency on the morphology of hair cells and auditory neurons, we examined sagittal sections from the inner ears of 4-month-old wild-type and *sirtaki* mice that carry a deletion mutation (p.K290X) in the *Pjvk* gene, abrogating the pejvakin C-terminal domain (Schwander et al., 2007b). We observed profound degenerative changes in the basal turn of the mutant cochlea (Fig. 2A and B) including the loss of hair cells (arrowheads) and a reduction in the density of spiral ganglion neurons (arrows). We next analyzed the cochlear sensory epithelia of homozygous and heterozygous *sirtaki* mice by immunofluorescence staining with an antibody to myosin VIIa and DAPI to label hair cells and nuclei, respectively. A detailed survey of the most basal region of the cochlea in homozygous *sirtaki* mice at P30 revealed scattered loss of OHCs (Fig. 2C–F; arrowheads), whereas IHCs were largely preserved (Fig. 2G, H). Quantification of the number of myosin VIIa-positive hair cells confirmed that the OHC density (cells per 100 micron) is significantly decreased in basal regions of the mutant cochlea (16 ± 7 OHCs/100 μm, mean ± SEM, $p < 0.05$, two-tailed *t* test) compared to heterozygous controls (39 ± 1 OHCs/100 μm) at this age (Fig. 2I). These results point to a critical role of the C-terminal domain of pejvakin in maintaining the integrity of sensory hair cells and possibly auditory neurons.

Function and morphology of IHC ribbon synapses is preserved in *sirtaki* mice

Because p.T54I and p.R183W mutations in *Pjvk* have been linked to ANSD (Delmaghani et al., 2006), we next asked whether pejvakin regulates synaptic transmission at the IHC ribbon synapse. To analyze the presynaptic function of IHCs we performed patch-clamp recordings of Ca^{2+} currents and exocytosis in *sirtaki* and age-matched control mice. We first examined the Ca^{2+}current that is largely mediated by $Ca_V1.3$ channels (Platzer et al., 2000; Brandt et al., 2003; Dou et al., 2004). No significant changes in the voltage-dependence were observed (the potential of half activation: −27.8 ± 1.1 vs. −30.4 ± 1.6 mV ($p = 0.2$, *Student's t test*); and the slope factor: 6.4 ± 0.1 mV vs. 5.9 ± 0.2 mV ($p = 0.1$, *Wilcoxon rank-sum test*) in IHCs of wild-type and *sirtaki* mice, respectively, as obtained by Boltzmann fits to the current-voltage relationships, see Experimental Procedures), while Ca^{2+} current amplitudes were slightly increased in the mutant mice (Fig. 3A). Likewise, a small increase in Ca^{2+} current inactivation was detected in mutant IHCs (Fig. 3B, C). We next analyzed depolarization-induced exocytosis using capacitance (C_m)measurements in perforated-patch recordings from IHCs in the cochlea of 2–3-week-old *sirtaki* and wild-type mice. Membrane capacitance (C_m) increments reflecting exocytosis were similar in IHCs of *sirtaki* and wild-type mice (Fig. 3) both for short stimuli (up to 20-ms depolarization: fusion of the readily releasable pool of vesicles, Fig. 3D) and for longer depolarizations (likely reporting vesicle replenishment and subsequent fusion, Fig. 3E). We further evaluated the integrity of IHC ribbon synapses in cochlear whole mount stainings with antibodies against the presynaptic ribbon protein Ribeye/CtBP2 and the postsynaptic glutamate receptor GluA 2/3 (Khimich et al., 2005). The number of synapses in mutant IHCs (Fig. 3F) was comparable to that of wild-type IHCs (Fig. 3G), while the overall number of ribbons and GluA receptor immunospots was slightly decreased (Table 1). Thus, in agreement with a previous study

(Delmaghani et al., 2015), we find that the electrophysiological and morphological properties of IHC synapses are largely unaffected in pejvakin mutant mice.

Hearing loss and hair cell degeneration in mice lacking pejvakin in OHCs

Based on the morphological defects observed in *sirtaki* mice, we hypothesized that pejvakin might primarily regulate the function of OHCs. To compare the effect of pejvakin deficiency in all hair cells or only in OHCs on auditory function, we crossed the tamoxifen-inducible hair cell-specific *Atoh1-CreER™* and OHC-specific *Prestin-CreER*^{T2} mouse lines with a conditional *pejvakin* allele (*Pjvk*$^{fl/fl}$) in which the first coding exon of the *Pjvk* gene is flanked by loxP sites (*Pjvk*$^{fl/fl}$ mice will be described in detail elsewhere) and performed neonatal tamoxifen injections (Experimental Procedures). We first verified the Cre-mediated recombination pattern in cochlear sensory epithelia by crossing the *Atoh1-CreER™* and *Prestin-CreER*^{T2} transgenic lines to Ai9 tdTomato Cre reporter mice (The Jackson Laboratory) (Madisen et al., 2010). In the early postnatal (P5) cochlea, *Atoh1-CreER™*-mediated recombination was observed in all hair cells following tamoxifen injections at P0 and P1 (Fig. 4A, C). In *Prestin-CreER*^{T2} mice, treated with tamoxifen (at P2, P3 and P4), many OHCs showed robust reporter activity at P7 whereas no Cre activity was detected in IHCs (Fig. 4B, D).

We next investigated the contribution of OHC defects to hearing loss in pejvakin mutant mice by comparing click-evoked auditory brainstem responses (ABRs) in *Pjvk*$^{fl/fl}$*Atoh1-CreER™*, *Pjvk*$^{fl/fl}$*Prestin-CreER*^{T2} and control mice (*Pjvk*$^{fl/+}$*Atoh1-CreER™*, *Pjvk*$^{fl/+}$*Prestin-CreER*^{T2}) subjected to the aforementioned tamoxifen regimens. At 1 month of age, click-ABR thresholds were highly increased in tamoxifen-treated homozygous *Pjvk*$^{fl/fl}$*Atoh1-CreER™* mice (83 ± 4 dB SPL, $n = 6$, mean ± SEM, $p<0.001$, two-tailed *t*-test) compared to heterozygous *Pjvk*$^{fl/+}$*Atoh1-CreER™* littermate controls (33 ± 3 dB SPL, $n = 7$) (Fig. 4E). No significant differences were found in ABR thresholds between untreated *Pjvk*$^{fl/fl}$*Atoh1-CreER™* mice (30 ± 2 dB SPL, $n = 7$) and untreated heterozygous littermates (32 ± 2 dB SPL, $n = 6$, $p > 0.4$, two-tailed *t*-test) (Fig. 4E). At 2 months, tamoxifen-treated *Pjvk*$^{fl/fl}$*Atoh1-CreER™* mice were profoundly hearing impaired with ABR thresholds exceeding 90 dB SPL ($n = 6$) (Fig. 4E, arrow). Analysis of ABR thresholds in *Pjvk*$^{fl/fl}$*Prestin-CreER*^{T2} mice (with neonatal tamoxifen injection) revealed a severity and progression of hearing impairment remarkably similar to the auditory phenotype of *Pjvk*$^{fl/fl}$*Atoh1-CreER™* mice. ABR thresholds in tamoxifen-treated *Pjvk*$^{fl/fl}$*Prestin-CreER*^{T2} mice were by 1 month at 89.2 ± 3.0 dB SPL ($n = 6$, mean ± SEM, $p < 0.005$, two-tailed t-test) compared to heterozygous controls 31.3 ± 2.3 dB SPL ($n = 8$) and by 2 months > 90 dB SPL (Fig. 4F). Slightly elevated thresholds were also observed in tamoxifen-treated heterozygous *Pjvk*$^{fl/+}$*Prestin-CreER*^{T2} mice ($p < 0.05$, $n = 5$, compared to untreated mice of the same genotype (n = 4)), which may be due to low levels of Cre-mediated toxicity (Forni et al., 2006).

To evaluate survival of hair cells we stained cochlear whole mounts from *Pjvk*$^{fl/fl}$*Atoh1-CreER™*, *Pjvk*$^{fl/fl}$*Prestin-CreER*^{T2} and control mice (*Pjvk*$^{fl/+}$*Atoh1-CreER™*, all 3 lines with neonatal tamoxifen injection) with a myosin VIIa antibody. By fluorescence microscopy, both IHCs and OHCs appeared normal in *Pjvk*$^{fl/+}$*Atoh1-CreER™* mice at P60

(Fig. 5A, D, G). In *Pjvk*$^{fl/fl}$*Atoh1-CreER™* mice however, there was a substantial loss of IHCs and OHCs in a basal to apical gradient along the cochlear duct (Fig. 5B, E, H). In the basal turn, OHCs were largely missing in all three rows, while a few IHCs were still preserved (Fig. 5H). By contrast, IHCs in *Pjvk*$^{fl/fl}$*Prestin-CreER*^{T2} mice appeared largely intact, and OHC loss was mostly confined to the medial and basal turns of the cochlea (Fig. 5C, F, I). The quantification of hair cell loss in *Pjvk*$^{fl/fl}$*Atoh1-CreER™* mice and their heterozygous littermates (Fig. 5J) revealed a significant decrease in the density of OHCs throughout the cochlea that was most pronounced in the basal turn (95 ± 3%, $p < 0.001$, n = 3–4, two-tailed t-test), while the density of IHCs was only significantly reduced at the cochlear base (76 ± 3%, $p < 0.05$). Importantly, *Pjvk*$^{fl/fl}$*Prestin-CreER*^{T2} mice (Fig. 5K) exhibited significant, 69 ± 4 and 88 ± 7% decreases in OHC density only in mid-basal and basal cochlea, respectively ($p < 0.001$ and $p < 0.05$, two-tailed t test, n = 3–4). The more restricted pattern of OHC degeneration in *Pjvk*$^{fl/fl}$*Prestin-CreER*^{T2} mice (Fig 5C, F, I, K) could be explained by differences in the onset of Cre activity between the two Cre mouse lines. Nevertheless, our data suggest that the presence of pejvakin in OHCs is essential for their survival.

To determine whether functional defects in OHCs are present prior to hair cell degeneration, we recorded distortion product otoacoustic emissions (DPOAEs), which are distortions of the sound input created and amplified by normally functioning OHCs that can be recorded by a microphone from the ear canal (Kemp, 2002a). At P17, DPOAE thresholds were highly elevated in tamoxifen-treated (at P2, P3 and P4) *Pjvk*$^{fl/fl}$*Prestin-CreER*^{T2} mice at all frequencies tested (for 16 kHz stimulus: 57 ± 3 dB SPL (n =4) versus 18 ± 1 dB SPL (n =4) control littermates, $p < 0.001$, two-tailed t-test) (Fig. 6A). To quantify OHC loss, we sacrificed the mice after auditory testing and stained cochlear whole mounts with a myosin VIIa antibody to visualize hair cells. No significant differences in the morphology (Fig. 6B) and density ($p > 0.05$, two-tailed t-test) (Fig. 6C) of OHCs were observed at this age. Since DPOAEs depend on the mechanical activity of OHCs, the data indicate that functional defects in OHCs precede hair cell degeneration in *Pjvk*$^{fl/fl}$*Prestin-CreER*^{T2} mice.

Pejvakin in adult OHCs is critical for normal hearing in mice

Hearing loss with either intact or absent OAEs has been reported in DFNB59 patients carrying the p.R183W mutation (Collin et al., 2007b), indicating that more subtle mutations in pejvakin may cause OHCs to degenerate over time. These findings together with the recently proposed role of noise in the etiology of DFNB59 (Delmaghani et al., 2015) prompted us to examine the degree to which changes in pejvakin activity in adult OHCs may affect auditory function. We therefore treated *Pjvk*$^{fl/fl}$*Prestin-CreER*^{T2} mice with tamoxifen at P21 and P22, a time when hair cells in the cochlea are functionally mature, and recorded ABRs at different ages. Following tamoxifen injections, robust tdTomato signal was detected in OHCs throughout the cochlea of *Prestin-CreER*^{T2}; Ai9 mice at P30 (Fig. 7A–C). Heterozygous (*Pjvk*$^{fl/+}$*Prestin-CreER*^{T2}) littermates had normal click- and pure-tone-evoked ABR thresholds at 1, 2, 4, and 7 months of age (Fig. 7D, E). ABR thresholds in 1-month-old *Pjvk*$^{fl/fl}$*Prestin-CreER*^{T2} mice did not differ significantly from the heterozygous controls (click-ABR: 35 ± 3 versus 41 ± 5 dB SPL ($p > 0.05$, two-tailed t-test) in homozygous and heterozygous mutant mice, respectively) (Fig. 7D, E). However, at 2 months of age,

homozygous mutant mice had slightly elevated ABR thresholds (click-ABR: 75 ± 3 dB SPL) compared to heterozygous littermates (37 ± 4 dB SPL, $p < 0.01$, two-tailed *t*-test) and the difference progressively increased with age (Fig. 7D, E). By 7 months, homozygotes had profound hearing loss across all frequencies (Fig. 7E). We conclude that the auditory phenotype in *Pjvk*$^{fl/fl}$*Prestin-CreER*^{T2} mice is progressive in nature and affects all tested frequencies.

Whole mount staining of organs of Corti revealed that many OHCs and IHCs were missing throughout the cochlea of homozygous (Fig. 7I–K) but not heterozygous (Fig. 7F–H) mutant mice at this age. Quantification of hair cell densities revealed that OHCs were lost to a greater extent than IHCs in the mutant cochlea (Apex: 88 ± 6% versus 51 ± 4% decreases in densities of OHCs and IHCs, respectively ($p < 0.05$, two-tailed *t*-test, $n = 3$ mice per group) (Fig. 7L). Differences observed in OHC density did not reach significance at the cochlear base because pronounced OHC loss in this region also occurred in some heterozygous mutants at this age. This is likely due to the C57BL/6J genetic background of the pejvakin mutant lines and its previously reported effects on hair cell loss (Spongr et al., 1997).

Pejvakin binds to ROCK2 and IQGAP1

To gain insight into the molecular pathways that are regulated by pejvakin in hair cells, we carried out yeast two-hybrid (Y2H) screens of a cochlear cDNA library (Zhao et al., 2014) using as bait either full length pejvakin or pejvakin C-terminal domain (aa 239–352). Despite high transformation efficiency, the full-length pejvakin bait only yielded 7 colonies on plates with quadruple dropout medium (SD/-Trp/-Leu/-His/-Ade) (Fig. 8A). This result may be explained by an autoinhibited conformation of pejvakin that precludes prey binding, as described for other gasdermins (Op de Beeck et al., 2011; Shi et al., 2015). Screens using pejvakin C-terminal domain (N-or C-terminally tagged with LexA) identified a larger number of transformants. All transformants were further tested for growth and blue color on plates with quadruple dropout medium (SD/-Trp/-Leu/-His/-Ade) and X-α-gal, yielding a total of 15 positive transformants (Fig. 8A). DNA sequence analysis of the inserts in the pGAD-HA library vector from these transformants revealed fragments corresponding to regions of ROCK2, an effector for the small GTPase Rho, and the scaffold protein IQGAP1, both well-known regulators of actin/microtubule dynamics (Amano et al., 1997; Bensenor et al., 2007; Le Clainche et al., 2007) (Fig. 8B). A small group of centrosomal proteins was also identified in the screen (Fig. 8B). The two-hybrid interactions defined regions encompassing coiled-coil domains in ROCK2, IQGAP1 and several other candidate proteins as the putative binding sites for the pejvakin C-terminal domain (Fig. 8C*,* data not shown). In particular, the pejvakin interacting region of ROCK2 (aa 682–1056) overlaps with its predicted coiled-coil domain, which binds to scaffold proteins that may orient ROCK2 towards its substrates (Truebestein et al., 2015). IQGAP1 contains several putative coiled-coil specific IQGAP1 repeats just downstream of its calponin homology domain (CHD) (Fig. 8C), and the sequence of the identified Y2H clone overlaps with one of the repeats (Fig. 8C).

Since both ROCK2 and IQGAP1 interacted with pejvakin in Y2H screens, we next asked whether they also form protein complexes *in vitro*. We therefore prepared constructs

containing the N-terminal (aa 1–240) or C-terminal (aa 241–352) domains of pejvakin fused to GFP (Gsdm-PJVK-GFP and GFP-PJVK-C-term) or FLAG-epitope tag (Gsdm-PJVK-FLAG and FLAG-PJVK-C-term) as well as GFP-tagged IQGAP1. When co-expressed in HeLa cells, Gsdm-PJVK-FLAG and IQGAP1-GFP co-localized along cortical actin filaments around the cell periphery (Fig. 9A). Some overlap of fluorescent signals was also observed between IQGAP1-GFP and C-term pejvakin-FLAG (Fig. 9B), while no co-localization was detected with phosphoglycerate kinase 1 (PGK1)-FLAG (Fig. 9C), which served as a negative control. We next coexpressed the FLAG-tagged N- and C-terminal domains of pejvakin together with GFP-tagged IQGAP1 or PGK1 in HEK293 cells and performed co-immunoprecipitation assays. GFP-IQGAP1 co-precipitated with the N-terminal domain of pejvakin (Fig. 9D, arrowhead) and, to a lesser extent, with its C-terminal domain (Fig 9E, arrowhead), but not with PGK1. We also prepared an HA-tagged version of ROCK2 (Leung et al., 1996) and tested for interactions with GFP-tagged pejvakin following its expression in HEK293 cells. The C-terminal domain of pejvakin bound efficiently to HA-ROCK2 (Fig. 9F, arrowhead) whereas no interaction could be detected with its N-terminal domain. Our data suggest that pejvakin associates with ROCK2 and other cytoskeletal signaling molecules mainly via its C-terminal domain.

Discussion

DFNB59 was initially characterized as auditory neuropathy (Delmaghani et al., 2006), while subsequent studies identified mutations in *PJVK* that cause hearing loss due to cochlear dysfunction, as evidenced by absent OAEs (Collin et al., 2007a; Ebermann et al., 2007; Schwander et al., 2007b). This indicates that diverse pathophysiological mechanisms underlie this disorder. The precise cell-type specific functions of pejvakin in the auditory system have not yet been fully resolved. Here, we demonstrate that pejvakin regulates OHC function and integrity in a cell-autonomous manner. Moreover, its activity in adult OHCs is essential for maintaining hair cell integrity and auditory function in mice. We found that both IHCs and OHCs degenerate in $Pjvk^{fl/fl}$*Atoh1-CreER™* mice that lack pejvakin specifically in hair cells, which is consistent with a recent report (Delmaghani et al., 2015). In these mice, scattered loss of IHCs and OHCs was evident throughout the cochlea at 2 months of age, but hair cell degeneration was more pronounced towards the cochlear base. By contrast, IHCs were less affected in mice lacking pejvakin only in OHCs and the degeneration of OHCs was mostly confined to the basal half of the cochlea. Surprisingly, hearing thresholds were equally and significantly elevated in both *Pjvk* conditional KO models at 1- and 2 months. Differences in the Cre-mediated recombination patterns between the two Cre lines may account for the more restricted pattern of OHC degeneration in $Pjvk^{fl/fl}$*Prestin-CreER*^{T2} mice, but they alone cannot explain the similarity of the auditory phenotypes. Thus, it seems likely that the similar increases in ABR thresholds (of about 50 dB) in $Pjvk^{fl/fl}$*Atoh1-CreER™* and $Pjvk^{fl/fl}$*Prestin-CreER*^{T2} mice are caused by functional in addition to morphological defects in OHCs. This interpretation is consistent with the reported 40- to 60-dB decrease of cochlear sensitivity in prestin mutant mice (Liberman et al., 2002) due to the loss of cochlear amplification by OHCs (Ryan and Dallos, 1975; Kharkovets et al., 2006). Indeed, we found that in tamoxifen-treated $Pjvk^{fl/fl}$*Prestin-CreER*^{T2} mice, DPOAE thresholds were highly elevated at all frequencies tested prior to

OHC loss. Our data thus suggest that OHC dysfunction is a major contributor to the hearing loss observed in mice and human patients carrying loss of function mutations in the *Pjvk* gene.

Another unexpected finding of our study is the slowly progressive hearing loss in mice induced by ablation of pejvakin in OHCs at P21, a time when cochlear function reaches maturity in the mouse. With respect to DFNB59, the idea that loss of function mutations in pejvakin may affect OHC function, leading to a decline of cochlear amplification and hearing sensitivity, is well established. *Sirtaki* mice develop early-onset progressive hearing loss and abnormal OAEs due to a C-terminal deletion mutation in *Pjvk* (Schwander et al., 2007b). Likewise, DFNB59 patients carrying nonsense mutations in *Pjvk* show a moderate to profound hearing loss that is progressive in nature (Ebermann et al., 2007; Schwander et al., 2007b). Progressive hearing loss has also been reported in patients carrying a p.C343S missense mutation, although OAEs were not assessed (Mujtaba et al., 2012). Lastly, abnormal OAEs were detected in individuals of a Turkish family (Collin et al., 2007a) carrying the same p.R183W mutation initially reported in Iranian families with ANSD (Delmaghani et al., 2006). These findings clearly suggest that pejvakin is critical for OHC function, although differences in genetic background, age of the tested individuals or, as recently suggested, in the exposures to noise (Delmaghani et al., 2015) might contribute to some of the observed phenotypic variabilities. We therefore propose that ANSD-linked mutations in the *Pjvk* gene may cause the disappearance of OAE responses over time, because, in our study, lack of pejvakin in adult OHCs led to a slow decline in hearing sensitivity. Indeed, OAEs are generally present in patients with ANSD, while in some cases they have been reported to be absent and/or changing over time (Berlin et al., 2010). Since no morphological defects in hair cells have been reported in p.R183W knock-in mice, it seems plausible that this ANSD-linked mutation may have a more subtle effect on pejvakin and either causes a slower progression of OHC degeneration and/or predominantly affects IHCs. It is currently unclear whether defects in IHCs contribute to the elevated ABR thresholds in DFNB59 patients with preserved OAEs. Our study shows that at least synaptic transmission at the IHC ribbon synapse is largely intact in *sirtaki* mice, in agreement with a previous report (Delmaghani et al., 2015).

Delmaghani et al. (2015) have indicated a critical role of pejvakin in peroxisome proliferation, as it occurs during noise exposure. Our study suggests another candidate molecular pathway of pejvakin, which involves the interaction of pejvakin with the Rho effector proteins ROCK2 and IQGAP1 that control actin nucleation and dynamics to alter cell shape (Amano et al., 1997; Bensenor et al., 2007; Le Clainche et al., 2007). Two independent ROCK2 clones were found to interact with pejvakin and were isolated a total of five times from the screen, while a single clone for IQGAP1 was isolated six times. ROCK2 is thought to anchor to the plasma membrane via its C-terminal PH domain, localizing its N-terminal kinase domain to substrates in the actin cortex through a long, central coiled-coil domain that acts as a molecular ruler (Shimizu et al., 2003; Truebestein et al., 2015). The coiled-coil domain may bind to scaffolding proteins that adjust the position of the coiled-coil and orient ROCK2 toward its substrates. Our study shows that the C-terminal domain of pejvakin interacts with the coiled-coil segment of ROCK2, suggesting a possible role for pejvakin in regulating ROCK2 kinase-substrate engagement. ROCK-mediated signaling

cascades have been implicated in modulating OHC electromotility by selectively targeting the cytoskeleton (Kalinec et al., 2000; Zhang et al., 2003). We show that DPOAEs, which depend on the mechanical activity of OHCs, are greatly reduced in mice lacking pejvakin specifically in OHCs. It will be interesting to determine in the future whether pejvakin is directly involved in this process or whether it regulates other aspects of cytoskeletal organization that are critical for OHC function.

Another candidate binding protein for pejvakin, the scaffold protein IQGAP1, is ubiquitously expressed and binds to F-actin via its N-terminal calponin homology domain (CHD) (Mateer et al., 2002; Brown and Sacks, 2006). The pejvakin interacting region overlaps with one of several putative coiled-coil specific IQGAP1 repeats (IR) that bind to the N-terminal FERM domain of ezrin, an interaction that may help position IQGAP1 at the cell cortex. Importantly, IQGAP2, a homolog of IQGAP1 with 62% similarity and a common domain structure, has been linked to age-related hearing impairment (ARHI) in a Finnish Saami population (Van Laer et al., 2010). This finding is particularly intriguing in view of the fact that certain mutations in pejvakin cause progressive hearing loss in mice and DFNB59 patients.

Conclusion

The results from our study demonstrate that pejvakin is required to sustain OHC activity and survival in a cell-autonomous manner and imply pejvakin defects in sensory hearing loss rather than ANSD. Based on our finding that inactivation of pejvakin in adult OHCs leads to progressive hearing loss, it is tempting to speculate that milder alleles of pejvakin may cause a slow degeneration of OHCs in adults while leaving hair cell development unaffected. Further, we show that pejvakin forms protein complexes with Rho effectors, including ROCK2, which has been implicated in the regulation of actin dynamics in OHCs (Kalinec et al., 2000; Zhang et al., 2003; Han et al., 2015). Understanding the effects of individual pejvakin mutations on Rho signaling may therefore shed light on the pathogenetic mechanisms that underlie the observed variability in clinical phenotypes in DFNB59 patients.

Acknowledgments

We thank Rixing Lin and other members of the Schwander laboratory for helpful discussions. We thank Bo Zhao for the cochlear cDNA library, Suzanne Baker for *Atoh1-CreER™* mice and Jian Zuo for *Prestin-CreER*^{T2} mice. We thank Thomas Leung, Manuela Baccarini and Tony Ng for ROCK2 constructs. The generation of the floxed *Pjvk* allele was carried out with funding from the NIDCD to Ulrich Mueller (DC014713, DC007704). This work was funded by NIH grant DC013331 (M.S), Rutgers the State University of New Jersey (M.S.), Busch Biomedical grant (M.S.), and a fellowship from the Capita Foundation for Hearing Research (M.S.) and the DFG through the collaborative research center 889 (TM).

References

Amano M, Chihara K, Kimura K, Fukata Y, Nakamura N, Matsuura Y, Kaibuchi K. Formation of actin stress fibers and focal adhesions enhanced by Rho-kinase. Science. 1997; 275:1308–1311. [PubMed: 9036856]

Bensenor LB, Kan HM, Wang N, Wallrabe H, Davidson LA, Cai Y, Schafer DA, Bloom GS. IQGAP1 regulates cell motility by linking growth factor signaling to actin assembly. Journal of cell science. 2007; 120:658–669. [PubMed: 17264147]

Berlin CI, Hood LJ, Morlet T, Wilensky D, Li L, Mattingly KR, Taylor-Jeanfreau J, Keats BJ, John PS, Montgomery E, Shallop JK, Russell BA, Frisch SA. Multi-site diagnosis and management of 260 patients with auditory neuropathy/dys-synchrony (auditory neuropathy spectrum disorder). International journal of audiology. 2010; 49:30–43. [PubMed: 20053155]

Brandt A, Striessnig J, Moser T. CaV1.3 channels are essential for development and presynaptic activity of cochlear inner hair cells. J Neurosci. 2003; 23:10832–10840. [PubMed: 14645476]

Brown MD, Sacks DB. IQGAP1 in cellular signaling: bridging the GAP. Trends in cell biology. 2006; 16:242–249. [PubMed: 16595175]

Chaleshtori MH, Farrokhi E, Shahrani M, Kheiri S, Dolati M, Rad LH, Pour-Jafari H, Samani KG, Chaleshtori KS, Crosby AH. High carrier frequency of the GJB2 mutation (35delG) in the north of Iran. International journal of pediatric otorhinolaryngology. 2007; 71:863–867. [PubMed: 17428550]

Chow LM, Tian Y, Weber T, Corbett M, Zuo J, Baker SJ. Inducible Cre recombinase activity in mouse cerebellar granule cell precursors and inner ear hair cells. Developmental dynamics : an official publication of the American Association of Anatomists. 2006; 235:2991–2998. [PubMed: 16958097]

Collin RW, Kalay E, Oostrik J, Caylan R, Wollnik B, Arslan S, den Hollander AI, Birinci Y, Lichtner P, Strom TM, Toraman B, Hoefsloot LH, Cremers CW, Brunner HG, Cremers FP, Karaguzel A, Kremer H. Involvement of DFNB59 mutations in autosomal recessive nonsyndromic hearing impairment. Hum Mutat. 2007a; 28:718–723. [PubMed: 17373699]

Collin RW, Kalay E, Oostrik J, Caylan R, Wollnik B, Arslan S, den Hollander AI, Birinci Y, Lichtner P, Strom TM, Toraman B, Hoefsloot LH, Cremers CW, Brunner HG, Cremers FP, Karaguzel A, Kremer H. Involvement of DFNB59 mutations in autosomal recessive nonsyndromic hearing impairment. Hum Mutat. 2007b; 28:718–723. [PubMed: 17373699]

Dallos P. The active cochlea. J Neurosci. 1992; 12:4575–4585. [PubMed: 1464757]

Dallos P, Wu X, Cheatham MA, Gao J, Zheng J, Anderson CT, Jia S, Wang X, Cheng WH, Sengupta S, He DZ, Zuo J. Prestin-based outer hair cell motility is necessary for mammalian cochlear amplification. Neuron. 2008; 58:333–339. [PubMed: 18466744]

Delmaghani S, del Castillo FJ, Michel V, Leibovici M, Aghaie A, Ron U, Van Laer L, Ben-Tal N, Van Camp G, Weil D, Langa F, Lathrop M, Avan P, Petit C. Mutations in the gene encoding pejvakin, a newly identified protein of the afferent auditory pathway, cause DFNB59 auditory neuropathy. Nat Genet. 2006; 38:770–778. [PubMed: 16804542]

Delmaghani S, et al. Hypervulnerability to Sound Exposure through Impaired Adaptive Proliferation of Peroxisomes. Cell. 2015; 163:894–906. [PubMed: 26544938]

Dou H, Vazquez AE, Namkung Y, Chu H, Cardell EL, Nie L, Parson S, Shin HS, Yamoah EN. Null mutation of alpha1D Ca2+ channel gene results in deafness but no vestibular defect in mice. Journal of the Association for Research in Otolaryngology : JARO. 2004; 5:215–226. [PubMed: 15357422]

Ebermann I, Walger M, Scholl HP, Charbel Issa P, Luke C, Nurnberg G, Lang-Roth R, Becker C, Nurnberg P, Bolz HJ. Truncating mutation of the DFNB59 gene causes cochlear hearing impairment and central vestibular dysfunction. Hum Mutat. 2007; 28:571–577. [PubMed: 17301963]

Fang J, Zhang WC, Yamashita T, Gao J, Zhu MS, Zuo J. Outer hair cell-specific prestin-CreERT2 knockin mouse lines. Genesis. 2012; 50:124–131. [PubMed: 21954035]

Forni PE, Scuoppo C, Imayoshi I, Taulli R, Dastru W, Sala V, Betz UA, Muzzi P, Martinuzzi D, Vercelli AE, Kageyama R, Ponzetto C. High levels of Cre expression in neuronal progenitors cause defects in brain development leading to microencephaly and hydrocephaly. J Neurosci. 2006; 26:9593–9602. [PubMed: 16971543]

Graus-Porta D, Blaess S, Senften M, Littlewood-Evans A, Damsky C, Huang Z, Orban P, Klein R, Schittny JC, Muller U. Beta1-class integrins regulate the development of laminae and folia in the cerebral and cerebellar cortex. Neuron. 2001; 31:367–379. [PubMed: 11516395]

Han Y, Wang X, Chen J, Sha SH. Noise-induced cochlear F-actin depolymerization is mediated via ROCK2/p-ERM signaling. J Neurochem. 2015; 133:617–628. [PubMed: 25683353]

Kalinec F, Zhang M, Urrutia R, Kalinec G. Rho GTPases mediate the regulation of cochlear outer hair cell motility by acetylcholine. The Journal of biological chemistry. 2000; 275:28000–28005. [PubMed: 10862776]

Kazmierczak M, Harris SL, Kazmierczak P, Shah P, Starovoytov V, Ohlemiller KK, Schwander M. Progressive Hearing Loss in Mice Carrying a Mutation in Usp53. J Neurosci. 2015; 35:15582–15598. [PubMed: 26609154]

Kemp DT. Otoacoustic emissions, their origin in cochlear function, and use. Br Med Bull. 2002a; 63:223–241. [PubMed: 12324396]

Kemp DT. Otoacoustic emissions, their origin in cochlear function, and use. Br Med Bull. 2002b; 63:223–241. [PubMed: 12324396]

Kharkovets T, Dedek K, Maier H, Schweizer M, Khimich D, Nouvian R, Vardanyan V, Leuwer R, Moser T, Jentsch TJ. Mice with altered KCNQ4 K+ channels implicate sensory outer hair cells in human progressive deafness. The EMBO journal. 2006; 25:642–652. [PubMed: 16437162]

Khimich D, Nouvian R, Pujol R, Tom Dieck S, Egner A, Gundelfinger ED, Moser T. Hair cell synaptic ribbons are essential for synchronous auditory signalling. Nature. 2005; 434:889–894. [PubMed: 15829963]

Le Clainche C, Schlaepfer D, Ferrari A, Klingauf M, Grohmanova K, Veligodskiy A, Didry D, Le D, Egile C, Carlier MF, Kroschewski R. IQGAP1 stimulates actin assembly through the N-WASP-Arp2/3 pathway. The Journal of biological chemistry. 2007; 282:426–435. [PubMed: 17085436]

Leung T, Chen XQ, Manser E, Lim L. The p160 RhoA-binding kinase ROK alpha is a member of a kinase family and is involved in the reorganization of the cytoskeleton. Molecular and cellular biology. 1996; 16:5313–5327. [PubMed: 8816443]

Liberman MC, Gao J, He DZ, Wu X, Jia S, Zuo J. Prestin is required for electromotility of the outer hair cell and for the cochlear amplifier. Nature. 2002; 419:300–304. [PubMed: 12239568]

Madisen L, Zwingman TA, Sunkin SM, Oh SW, Zariwala HA, Gu H, Ng LL, Palmiter RD, Hawrylycz MJ, Jones AR, Lein ES, Zeng H. A robust and high-throughput Cre reporting and characterization system for the whole mouse brain. Nature neuroscience. 2010; 13:133–140. [PubMed: 20023653]

Mateer SC, McDaniel AE, Nicolas V, Habermacher GM, Lin MJ, Cromer DA, King ME, Bloom GS. The mechanism for regulation of the F-actin binding activity of IQGAP1 by calcium/calmodulin. The Journal of biological chemistry. 2002; 277:12324–12333. [PubMed: 11809768]

Moser T, Beutner D. Kinetics of exocytosis and endocytosis at the cochlear inner hair cell afferent synapse of the mouse. Proceedings of the National Academy of Sciences of the United States of America. 2000; 97:883–888. [PubMed: 10639174]

Moser T, Starr A. Auditory neuropathy - neural and synaptic mechanisms. Nature reviews Neurology. 2016; 12:135–149. [PubMed: 26891769]

Mujtaba G, Bukhari I, Fatima A, Naz S. A p.C343S missense mutation in PJVK causes progressive hearing loss. Gene. 2012; 504:98–101. [PubMed: 22617256]

Op de Beeck K, Van Camp G, Thys S, Cools N, Callebaut I, Vrijens K, Van Nassauw L, Van Tendeloo VF, Timmermans JP, Van Laer L. The DFNA5 gene, responsible for hearing loss and involved in cancer, encodes a novel apoptosis-inducing protein. European journal of human genetics : EJHG. 2011; 19:965–973. [PubMed: 21522185]

Platzer J, Engel J, Schrott-Fischer A, Stephan K, Bova S, Chen H, Zheng H, Striessnig J. Congenital deafness and sinoatrial node dysfunction in mice lacking class D L-type Ca2+ channels. Cell. 2000; 102:89–97. [PubMed: 10929716]

Roux I, Safieddine S, Nouvian R, Grati M, Simmler MC, Bahloul A, Perfettini I, Le Gall M, Rostaing P, Hamard G, Triller A, Avan P, Moser T, Petit C. Otoferlin, defective in a human deafness form, is essential for exocytosis at the auditory ribbon synapse. Cell. 2006; 127:277–289. [PubMed: 17055430]

Ruel J, Emery S, Nouvian R, Bersot T, Amilhon B, Van Rybroek JM, Rebillard G, Lenoir M, Eybalin M, Delprat B, Sivakumaran TA, Giros B, El Mestikawy S, Moser T, Smith RJ, Lesperance MM, Puel JL. Impairment of SLC17A8 encoding vesicular glutamate transporter-3, VGLUT3, underlies nonsyndromic deafness DFNA25 and inner hair cell dysfunction in null mice. American journal of human genetics. 2008; 83:278–292. [PubMed: 18674745]

Ryan A, Dallos P. Effect of absence of cochlear outer hair cells on behavioural auditory threshold. Nature. 1975; 253:44–46. [PubMed: 1110747]

Saeki N, Kuwahara Y, Sasaki H, Satoh H, Shiroishi T. Gasdermin (Gsdm) localizing to mouse Chromosome 11 is predominantly expressed in upper gastrointestinal tract but significantly suppressed in human gastric cancer cells. Mamm Genome. 2000; 11:718–724. [PubMed: 10967128]

Schoen CJ, Emery SB, Thorne MC, Ammana HR, Sliwerska E, Arnett J, Hortsch M, Hannan F, Burmeister M, Lesperance MM. Increased activity of Diaphanous homolog 3 (DIAPH3)/diaphanous causes hearing defects in humans with auditory neuropathy and in Drosophila. Proceedings of the National Academy of Sciences of the United States of America. 2010; 107:13396–13401. [PubMed: 20624953]

Schwander M, Sczaniecka A, Grillet N, Bailey JS, Avenarius M, Najmabadi H, Steffy BM, Federe GC, Lagler EA, Banan R, Hice R, Grabowski-Boase L, Keithley EM, Ryan AF, Housley GD, Wiltshire T, Smith RJ, Tarantino LM, Muller U. A forward genetics screen in mice identifies recessive deafness traits and reveals that pejvakin is essential for outer hair cell function. J Neurosci. 2007a; 27:2163–2175. [PubMed: 17329413]

Schwander M, Sczaniecka A, Grillet N, Bailey JS, Avenarius M, Najmabadi H, Steffy BM, Federe GC, Lagler EA, Banan R, Hice R, Grabowski-Boase L, Keithley EM, Ryan AF, Housley GD, Wiltshire T, Smith RJ, Tarantino LM, Muller U. A forward genetics screen in mice identifies recessive deafness traits and reveals that pejvakin is essential for outer hair cell function. J Neurosci. 2007b; 27:2163–2175. [PubMed: 17329413]

Senften M, Schwander M, Kazmierczak P, Lillo C, Shin JB, Hasson T, Geleoc GS, Gillespie PG, Williams D, Holt JR, Muller U. Physical and functional interaction between protocadherin 15 and myosin VIIa in mechanosensory hair cells. J Neurosci. 2006; 26:2060–2071. [PubMed: 16481439]

Shi J, Zhao Y, Wang K, Shi X, Wang Y, Huang H, Zhuang Y, Cai T, Wang F, Shao F. Cleavage of GSDMD by inflammatory caspases determines pyroptotic cell death. Nature. 2015; 526:660–665. [PubMed: 26375003]

Shimizu T, Ihara K, Maesaki R, Amano M, Kaibuchi K, Hakoshima T. Parallel coiled-coil association of the RhoA-binding domain in Rho-kinase. The Journal of biological chemistry. 2003; 278:46046–46051. [PubMed: 12954645]

Spongr VP, Flood DG, Frisina RD, Salvi RJ. Quantitative measures of hair cell loss in CBA and C57BL/6 mice throughout their life spans. J Acoust Soc Am. 1997; 101:3546–3553. [PubMed: 9193043]

Starr A, Picton TW, Sininger Y, Hood LJ, Berlin CI. Auditory neuropathy. Brain. 1996; 119(Pt 3): 741–753. [PubMed: 8673487]

Truebestein L, Elsner DJ, Fuchs E, Leonard TA. A molecular ruler regulates cytoskeletal remodelling by the Rho kinases. Nature communications. 2015; 6:10029.

Van Laer L, Huyghe JR, Hannula S, Van Eyken E, Stephan DA, Maki-Torkko E, Aikio P, Fransen E, Lysholm-Bernacchi A, Sorri M, Huentelman MJ, Van Camp G. A genome-wide association study for age-related hearing impairment in the Saami. European journal of human genetics : EJHG. 2010; 18:685–693. [PubMed: 20068591]

Varga R, Kelley PM, Keats BJ, Starr A, Leal SM, Cohn E, Kimberling WJ. Non-syndromic recessive auditory neuropathy is the result of mutations in the otoferlin (OTOF) gene. Journal of medical genetics. 2003; 40:45–50. [PubMed: 12525542]

Warr WB, Guinan JJ Jr. Efferent innervation of the organ of corti: two separate systems. Brain research. 1979; 173:152–155. [PubMed: 487078]

Wichmann C, Moser T. Relating structure and function of inner hair cell ribbon synapses. Cell and tissue research. 2015; 361:95–114. [PubMed: 25874597]

Zhang M, Kalinec GM, Urrutia R, Billadeau DD, Kalinec F. ROCK-dependent and ROCK-independent control of cochlear outer hair cell electromotility. The Journal of biological chemistry. 2003; 278:35644–35650. [PubMed: 12837763]

Zhang QJ, Lan L, Li N, Qi Y, Zong L, Shi W, Yu L, Wang H, Yang J, Xie LY, Zhao F, Wang DY, Han B, Wang QJ. Identification of a novel mutation of PJVK in the Chinese non-syndromic hearing

loss population with low prevalence of the PJVK mutations. Acta oto-laryngologica. 2015; 135:211–216. [PubMed: 25631766]

Zhao B, Wu Z, Grillet N, Yan L, Xiong W, Harkins-Perry S, Muller U. TMIE is an essential component of the mechanotransduction machinery of cochlear hair cells. Neuron. 2014; 84:954–967. [PubMed: 25467981]

Zheng J, Shen W, He DZ, Long KB, Madison LD, Dallos P. Prestin is the motor protein of cochlear outer hair cells. Nature. 2000; 405:149–155. [PubMed: 10821263]

Highlights

- Mutations in *pejvakin* cause auditory neuropathy or hair cell-related deafness
- We have tested the cell-type specific functions of pejvakin in the auditory system
- Lack of pejvakin in all hair cells or in outer hair cells causes profound deafness
- Pejvakin is critical for adult outer hair cells but not inner hair cell synapses
- Pejvakin forms a complex with the Rho effectors ROCK2 and IQGAP1

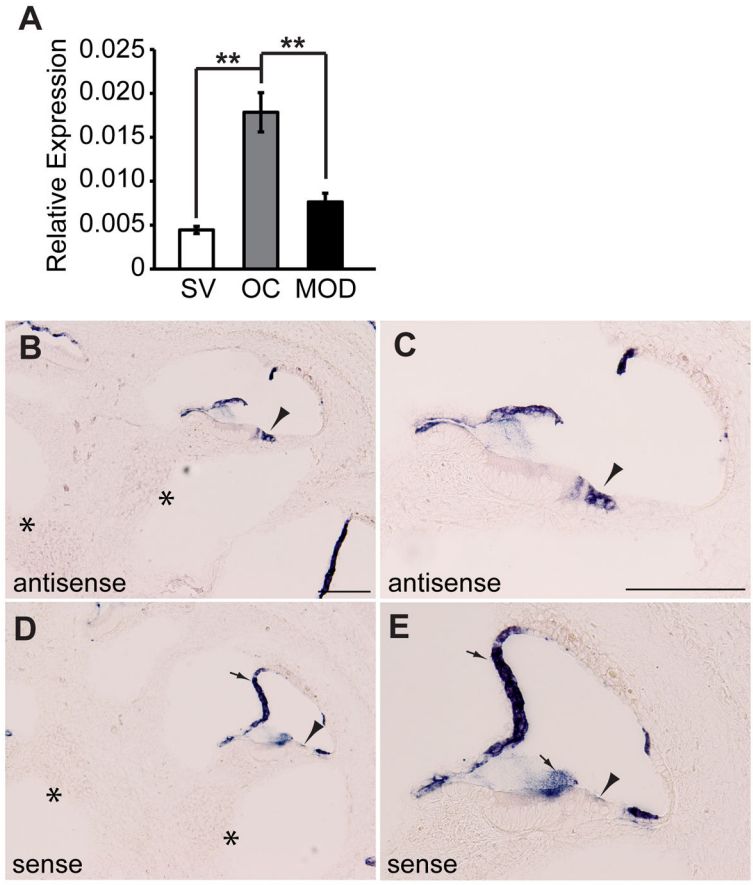

Figure 1. Hair cell expression of *Pjvk*

(A) Quantitative-PCR analysis of *Pjvk* in RNA extracted from inner ear tissues at P5. mRNA levels of *Pjvk* in stria vascularis (SV), organ of Corti (OC) and modiolus (MOD) were quantified in relation to the housekeeping gene *Pgk1*. All values are mean ± SEM ($n = 4$ mice; $^{**}p < 0.01$, two-tailed *t*-test). (B–E) Analysis of *Pjvk* expression by in situ hybridization on P4 inner ear sections. *Pjvk* is selectively expressed in cochlear hair cells (B, C, arrowheads), but there was no detectable signal in spiral ganglion neurons (B, asterisks). Nonspecific hybridization signal in the tectorial membrane and Reissner's membrane was also observed in sections incubated with a *Pjvk* sense probe (D, E, arrows), which served as a negative control. No signal was seen in either hair cells (arrowheads) or auditory neurons (asterisks). Scale bars: (in B and C) B–E, 100 μm.

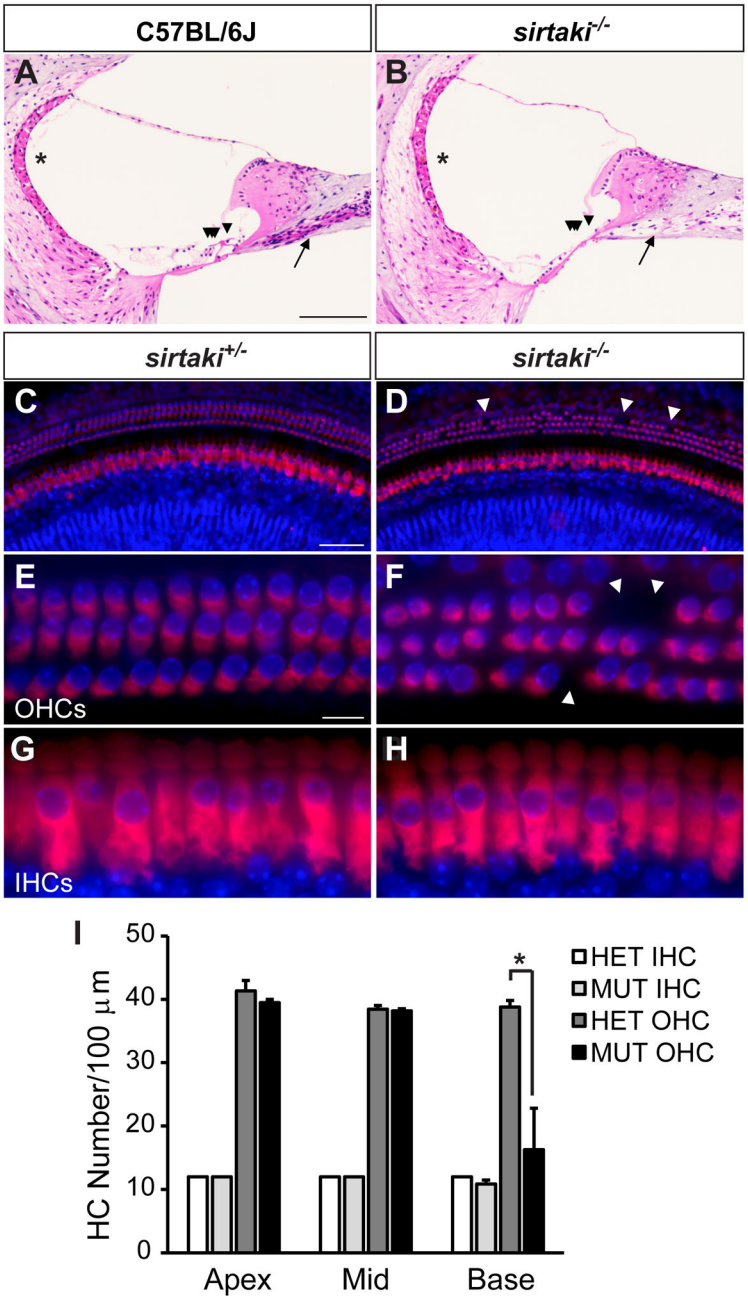

Figure 2. Hair cell degeneration in *Pjvk* mutant mice

(A, B) Sagittal inner ear sections from 4-month-old C57BL/6J wild-type (A) and *sirtaki* mutant (B) mice were stained with hematoxylin-eosin. Severe degeneration of hair cells in the organ of Corti (arrowheads) and spiral ganglion neurons (arrows) was evident in mutant but not in wild-type mice. No structural abnormalities of the stria vascularis were noted (asterisks). (C–H) Whole mounts from the basal turn of the cochleae from P30 littermate heterozygous (C, E, G) and homozygous (D, F, H) *sirtaki* mice were stained with an antibody against myosin VIIa and DAPI to label hair cells and nuclei, respectively. Note that sporadic missing OHCs (D, F, arrowheads) can be seen in the basal turn while IHCs are

preserved. (I) Quantification of hair cell density in each cochlear turn of P30 heterozygous (HET; $n = 3$) and homozygous (MUT; $n = 3$) *sirtaki* mice (mean ± SEM, $*p < 0.05$, Student's *t*-test). Scale bars: (in A) A, B, 80 μm; (in C) C, D, 50 μm; (in E) E–H, 10 μm.

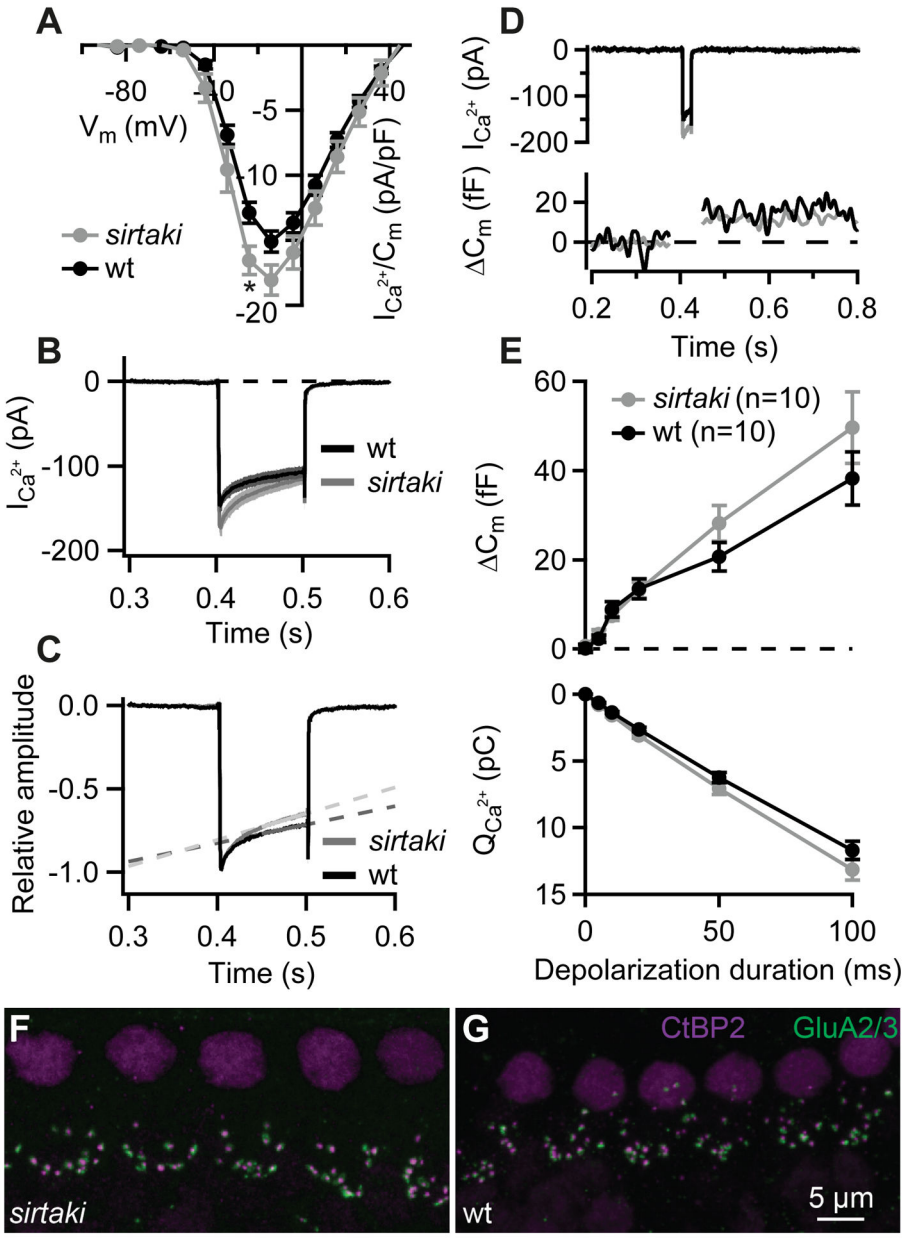

Figure 3. Synaptic function of IHCs is preserved in *sirtaki* mice carrying a C-terminal deletion in pejvakin

(A) Current-voltage relationship of the voltage-gated Ca^{2+} current normalized to the cell membrane capacitance in *sirtaki* (grey; $n = 10$) and wild-type control (black; $n = 10$) IHCs from 2–3-week-old mice. In the mutant IHCs Ca^{2+} current densities were slightly larger (*, Student's *t*-test, $p = 0.02$). (B–C) Absolute (B) and normalized (C) Ca^{2+} currents in response to 100-ms depolarizations to the peak Ca^{2+} current potential. Note a stronger Ca^{2+}-current inactivation in the mutant IHCs. In 100 ms, Ca^{2+} current was reduced for 23 ± 1 and 30 ± 2% in wild-type ($n = 10$) and mutant ($n = 10$) IHCs, respectively (calculated as the ratio of the final and initial calcium current amplitude, $I_{final}/I_{initial}$; $p = 0.005$, Student's *t*-test). The slope of the linear fit (1/s) to the Ca^{2+} currents in wild-type ($n = 10$) and mutant ($n = 10$)

IHCs had a value of 1.1 ± 0.1 and 1.6 ± 0.1, respectively ($p = 0.002$, Student's *t*-test). (D) Representative Ca^{2+} currents (top) and membrane capacitance ($\Delta \mathbf{C}_m$) responses (bottom) evoked by 20-ms depolarization to peak Ca^{2+} current potential. (E) Exocytosis ($\Delta \mathbf{C}_m$, top) and the corresponding Ca^{2+} current integrals (Q_{Ca}, bottom) as a function of duration of depolarizations to the peak Ca^{2+} current potential. The C_m increases and Q_{Ca} are comparable in the mutant (grey) and the wild-type (black) IHCs ($p > 0.05$, Student's *t*-test and Wilcoxon rank-sum test). All responses are given as grand averages (calculated from the means of the individual cells) ± S.E.M. (F–G) Confocal images of whole-mounts of organs of Corti double stained for the presynaptic marker CtBP2/Ribeye (magenta) and postsynaptic marker GluA 2/3 (green). The number of synapses in mutant IHCs (F) was comparable to that of wild-type IHCs (G), however in total we observed fewer ribbons and fewer GluA receptor immunospots (see Table 1).

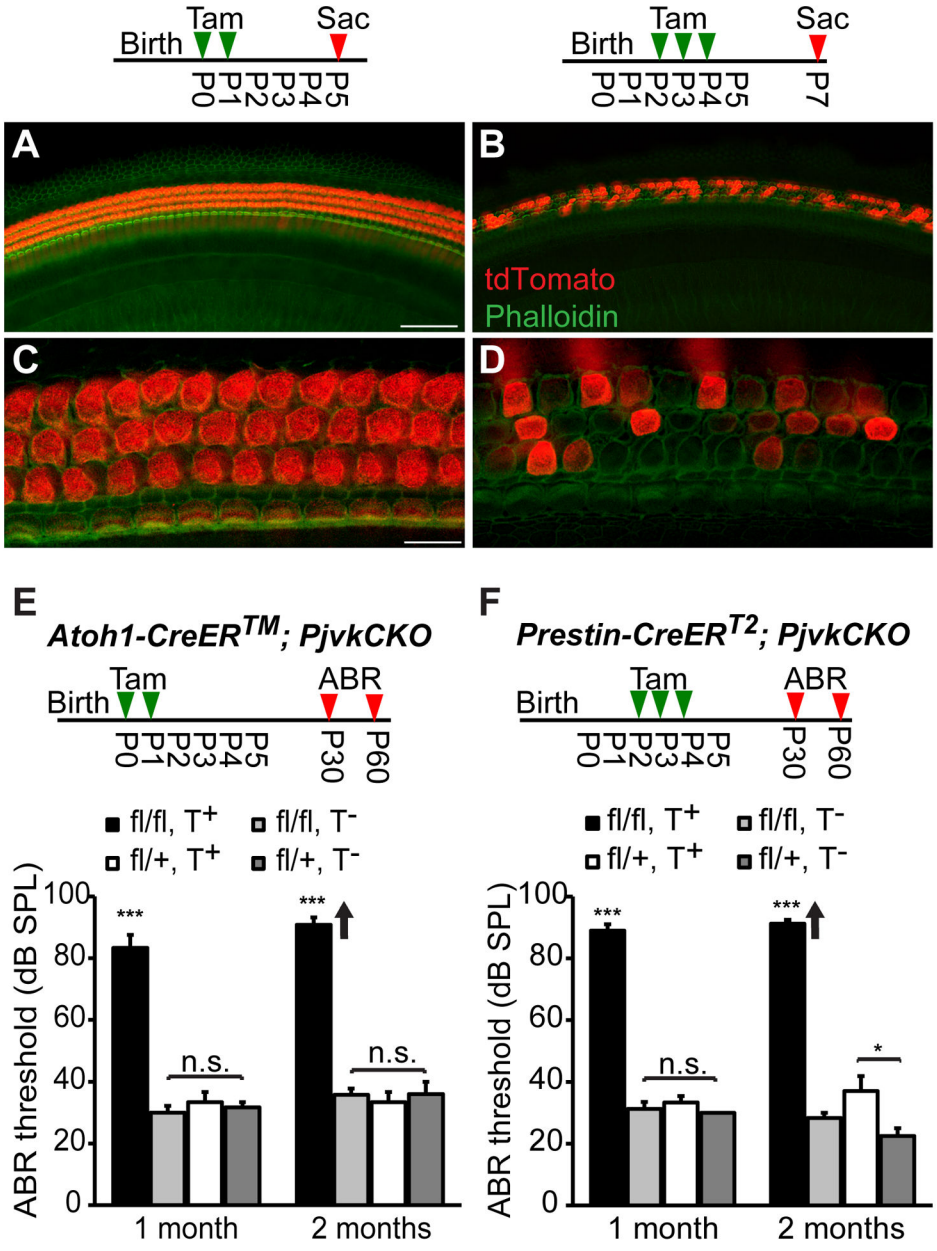

Figure 4. Hearing loss in *Atoh1-CreER™; Pjvk^{CKO}* and *Prestin-CreER^{T2}; Pjvk^{CKO}* mice

(A, C) Representative images of the cochlea from *Atoh1-CreER™*; Ai9 tdTomato mice at P5 following injections with tamoxifen (3mg/40g body weight) at P0 and P1. The timeline shows the protocol for tamoxifen injection (Tam) and cochlea collection (Sac). Note that tdTomato (red) is expressed in both IHCs and OHCs that are labeled with phalloidin (green). (B, D) Representative images of tdTomato expression in OHCs of tamoxifen-treated (at P2, P3 and P4) *Prestin-CreER^{T2}*; Ai9 tdTomato mice at P7. Note that mice are mosaic for tdTomato expression in OHCs at this age whereas no Cre activity was observed in IHCs. (E) Average click-ABR thresholds in tamoxifen-treated (T^+) and untreated (T^-) *Atoh1-CreER™Pjvk$^{fl/fl}$* (fl/fl) and *Atoh1-CreER™Pjvk$^{fl/+}$* (fl/+) mice at 1 and 2 months of age.

The timeline shows the protocol for tamoxifen injection (Tam) and ABR recordings (ABR). Data are presented as mean ± SEM. ***$p < 0.001$ (Student's *t*-test, $n \geq 4$ mice per group). Individual mice in the 2 months tamoxifen-treated mutant (fl/fl, T^+) group displayed auditory thresholds beyond the range of our measurements (>90 dB SPL). Arrows indicate that the mean thresholds are higher than shown on the graph. (F) Average click-ABR thresholds in tamoxifen-treated (T^+) and untreated (T^-) *Prestin-CreER*^{T2}*Pjvk*$^{fl/fl}$ (fl/fl) and *Prestin-CreER*^{T2}*Pjvk*$^{fl/+}$ (fl/+) mice at 1 and 2 months of age (*$p < 0.05$, ***$p < 0.001$, Student's *t*-test; $n \geq 4$ mice per group; mean ± SEM.). Scale bars: (in A) A, B, 50 μm; (in C) C, D, 10 μm.

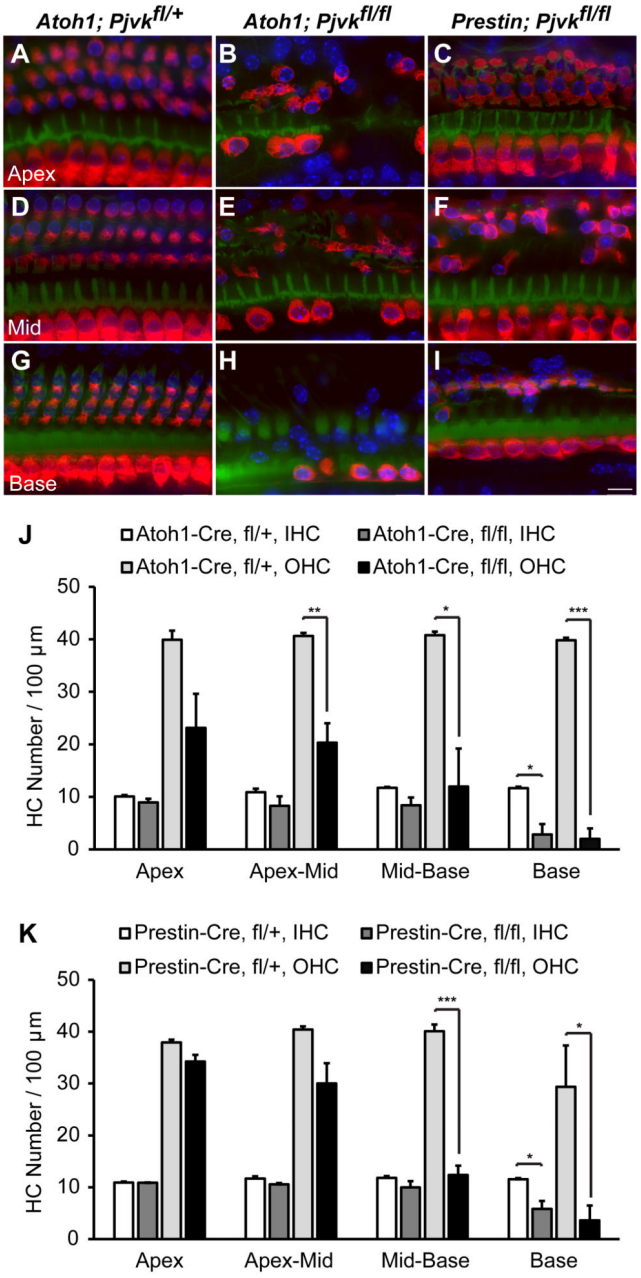

Figure 5. Hair cell degeneration in *Atoh1-CreER™; Pjvk^{CKO}* and *Prestin-CreER^{T2}; Pjvk^{CKO}* mice

(A–I) Cochlear whole mounts of tamoxifen-treated *Atoh1-CreER™Pjvk$^{fl/+}$*, *Atoh1-CreER™Pjvk$^{fl/fl}$* and *Prestin-CreER^{T2} Pjvk$^{fl/fl}$* mice at P60 were stained with phalloidin (F-actin, green), DAPI (nuclei, blue) and an antibody against myosin VIIa (red) to visualize hair cells. Apical, middle and basal cochlear turns for each genotype are shown. (J, K) Quantification of hair cell density in four different regions (apex, apex-mid, mid-base and base) along the cochlear sensory epithelium of tamoxifen-treated *Atoh1-CreER™; Pjvk^{CKO}* (J) and *Prestin-CreER^{T2}; Pjvk^{CKO}* (K) mice at P60. Data are presented as mean ± SEM. *p

< 0.05, *p < 0.01, ***p < 0.001 (Student's t-test, n = 3 mice per group). Scale bars: (in I) A–I, 10 μm.

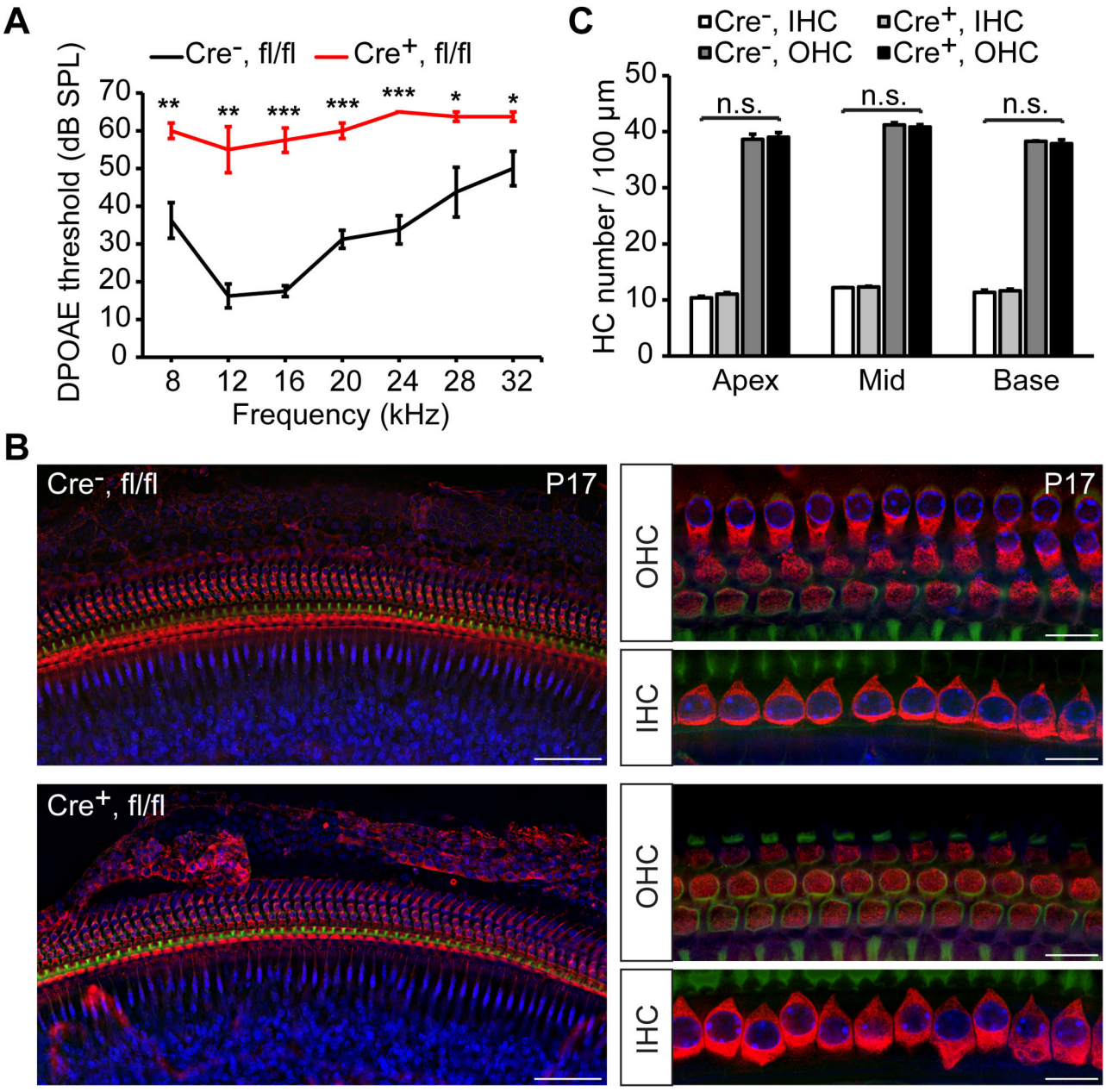

Figure 6. Analysis of DPOAEs in *Prestin-CreER*^{T2}; *Pjvk*^{CKO} mice

(A) Average DPOAE thresholds at different frequencies in tamoxifen-treated *Prestin-CreER*$^{T2+/-}$ *Pjvk*$^{fl/fl}$ mice (Cre^{+}, fl/fl; red) and *Prestin-CreER*$^{T2-/-}$ *Pjvk*$^{fl/fl}$ littermates (Cre^{-}, fl/fl; black) at P17. Data are presented as mean ± SEM. *$p < 0.05$, **$p < 0.01$, ***$p < 0.001$, (Student's *t*-test, $n = 4$ mice per group). (B) Whole-mount surface views at low (left panels) and high magnification (right panels) of the base of a Cre-positive (Cre^{+}, fl/fl) and Cre-negative (Cre^{+}, fl/fl) *Prestin-CreER*^{T2} *Pjvk*$^{fl/fl}$ cochlea at P17 immunolabeled with myosin VIIa antibody. (C) Quantification of hair cell numbers at P17 shows no significant changes in the density of OHCs in cochlea of Cre-positive (Cre^{+}) and Cre-negative (Cre^{-}) *Prestin-*

CreER^{T2} *Pjvk*$^{fl/fl}$ mice. Data are mean ± SEM (n = 3 cochleae from different mice per group; $p > 0.05$; Student's t-test).

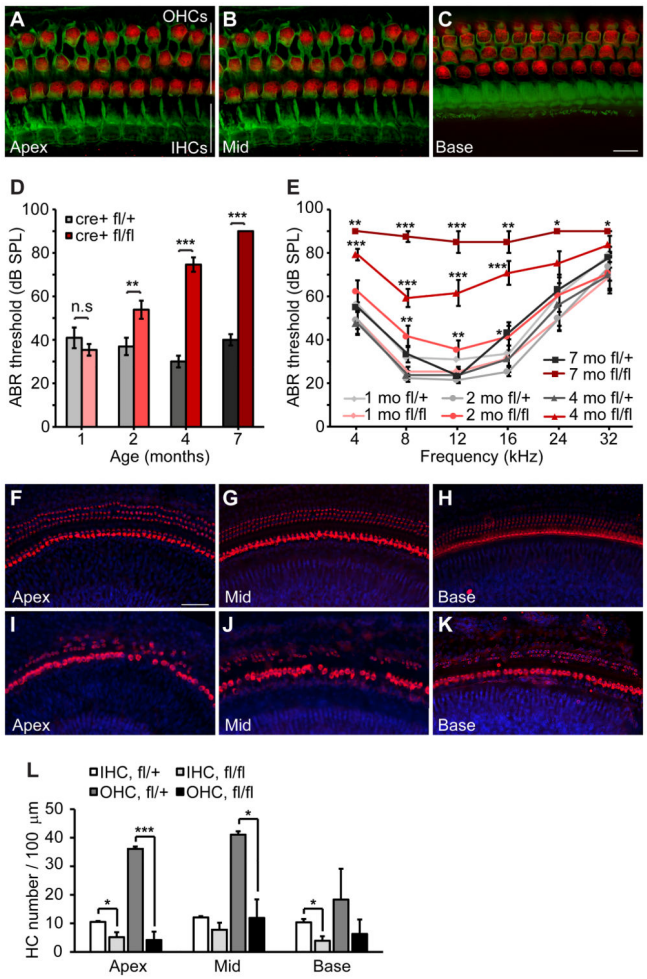

Figure 7. *Prestin-CreER*^{T2}-mediated pejvakin ablation in adult OHCs causes a slowly progressive hearing loss

(A–C) Representative images of whole mounts from the apical, medial and basal turns of the cochlea of tamoxifen-treated (at P21 and P22) *Prestin-CreER*^{T2}; Ai9 mice at P30 showing tdTomato^{+} OHCs (red) and F-actin (phalloidin, green). Note that tdTomato is not expressed in IHCs. (D) Average click-evoked ABR thresholds for 1, 2, 4, and 7-months-old *Prestin-CreER*^{T2}*Pjvk*$^{fl/fl}$ (cre+ fl/fl; $n = 13$) and *Prestin-CreER*^{T2}*Pjvk*$^{fl/+}$ (cre+ fl/+; $n = 11$) mice following tamoxifen injections at P21 and P22 (mean ± SEM; $^{**}p < 0.01$, $^{***}p < 0.001$; Student's *t*-test) (E) Average pure tone-evoked auditory thresholds for *Prestin-CreER*^{T2}*Pjvk*$^{fl/fl}$ (fl/fl; $n = 13$) and *Prestin-CreER*^{T2}*Pjvk*$^{fl/+}$ (fl/+; $n = 11$) mice subjected to the same tamoxifen regimens (mean ± SEM. $^{*}p < 0.05$, $^{**}p < 0.01$, $^{***}p < 0.001$, Student's *t*-test). (F–K) Cochlear whole mounts of tamoxifen-treated (at P21 and P22) 7-months-old *Prestin-CreER*^{T2}*Pjvk*$^{fl/+}$ (F–H) and *Prestin-CreER*^{T2}*Pjvk*$^{fl/fl}$ (I–K) mice were stained with an antibody against myosin VIIa (red) and DAPI (blue) to label hair cells and nuclei, respectively. (L) Quantification of hair cell density in the different regions of the cochlea of 7-months-old heterozygous (fl/+) and homozygous (fl/fl) *Prestin-CreER*^{T2}*Pjvk*$^{fl/+}$ mice. Data are mean ± SEM ($n = 3$ cochleae from different mice per group; $^{*}p < 0.05$, $^{***}p < 0.001$, Student's *t*-test). Scale bars: (in C) A–C, 10 µm; (in F), F–K, 50 µm.

A

Screen	Transformants	Colonies on SD-WLHA	ß-GAL+ colonies
PJVK-LexA	5.49 x 10^7	7	2
PJVK C-term-LexA	2.88 x 10^7	57	7
LexA-PJVK C-term	6.21 x 10^7	1501	6

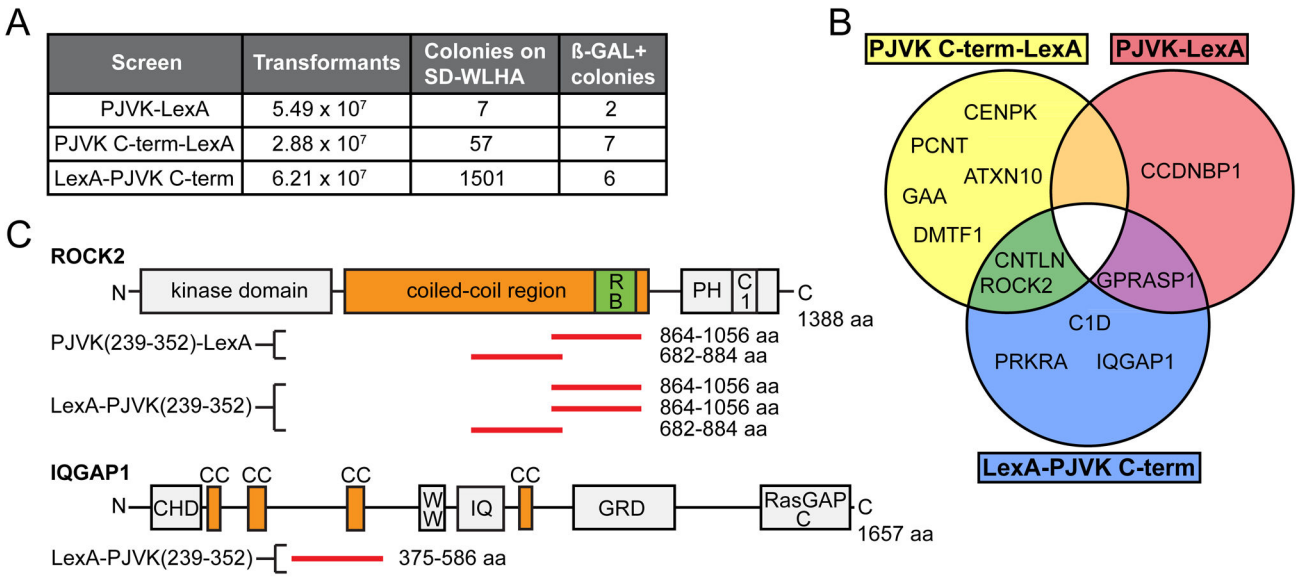

Figure 8. Interaction of pejvakin with cytoskeletal proteins in a yeast two-hybrid assay

(A) Summary of the number of transformants, clones that grew on quadruple dropout media (SD-WLHA), and clones verified for growth and blue color on SD-WLHA and X-α-gal media. The different bait constructs containing either full length or C-terminal domain of pejvakin are indicated in the left column. (B) Venn diagram illustrating the overlap between the three pejvakin binding candidates datasets described in this study. (C) Schematic representation of domains and motifs in ROCK2 and IQGAP1. In ROCK2, N-terminal kinase and C-terminal membrane-binding PH and C1 domains are separated by a predicted coiled-coil regions that contains the Rho-binding domain. Clones identified in the Y2H screen with pejvakin C-terminal domain are aligned relative to the sequence of ROCK2 (red bars). The pejvakin interacting region of ROCK2 (amino acids 682–1056) is located within the coiled-coil region of ROCK2. IQGAP1 contains an N-terminal calponin homology domain (CHD), putative coiled-coil domains (CC); a poly-proline protein-protein domain (WW), an IQ calmodulin binding motif (IQ), a rasGAP-related domain (GRD) and a C-terminal RasGAP domain (RasGAPc). The interacting region determined from the overlapping sequence of a Y2H clone is indicated (red bar). Abbreviations: Ccndbp1, cyclin D-type binding-protein 1; Gprasp, G protein-coupled receptor associated sorting protein 1; Cenpk, centromere protein K; Pcnt, pericentrin; ROCK2, Rho-associated coiled-coil containing protein kinase 2; Cntln, centlein; Gaa, glucosidase alpha acid; Atxn10, ataxin 10; Dmtf1, cyclin D binding myb-like transcription factor 1; C1d, C1D nuclear receptor co-repressor; IQGAP1, IQ motif containing GTPase activating protein 1; Prkra, protein kinase, interferon inducible double stranded RNA dependent activator.

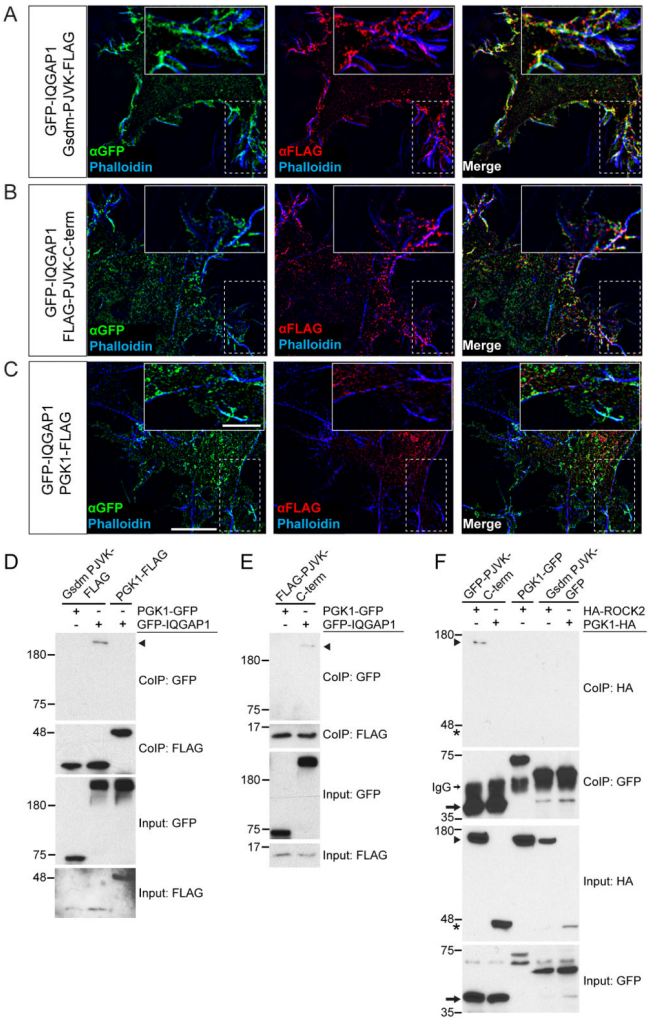

Figure 9. Interactions between pejvakin and Rho effectors

(A–C) HeLa cells were co-transfected with expression vectors for GFP-tagged IQGAP1 and FLAG-tagged pejvakin N- and C-terminal domains (PJVK) or PGK1-FLAG, which served as a negative control, and analyzed for protein localization one day after transfection. GFP-tagged IQGAP1 is shown in green, domains of PJVK and PGK1-FLAG in red. F-actin was labeled with phalloidin (blue). Scale bars: 10 μm, insets: 5 μm. (D, E) HEK293T cells were transfected with the constructs indicated on top of each panel. Immunoprecipitations were carried out with FLAG antibody followed by western blotting with GFP and FLAG antibodies to detect GFP-IQGAP1 (arrowhead) and bait proteins, respectively. The upper rows show CoIP results and the lower rows show input protein. (F) HEK293 cells were transfected with the constructs indicated on top of the panel. Immunoprecipitations were carried out with GFP antibody followed by western blotting with GFP and HA antibodies. Note that binding activity was detected between GFP-PJVK C-term (arrow) and HA-ROCK2 (arrowhead), while no binding was detected with PGK1-HA (asterisks).

Table 1

Quantification of ribbon synapses

Synapses were counted in IHCs of 2 organs of Corti of wild-type and 2 organs of Corti of *sirtaki* mice (for each genotype 82 IHCs were analyzed). Intact synapses were defined by the juxtaposition of pairs of pre- and postsynaptic fluorescent spots. The number of GluA receptors per cell includes the GluA receptors with and those without the presynaptic ribbon partner. The same applies to the number of ribbons given in the table. Data are shown as mean ± S.E.M., paired *t*-test.

	No. of synapses/cell		No. of ribbons/cell		No. of GluA/cell	
sirtaki	11.5 ± 0.6	$p = 0.2$	12.2 ± 0.5	$p = 0.049$	12.6 ± 0.1	$p = 0.002$
wild-type	12.7 ± 0.7		15.0 ± 0.8		14.2 ± 0.0	